# Modeling of Lead Halide Perovskites for Photovoltaic Applications

Radi A. Jishi,*,[†] Oliver B. Ta,[‡] and Adel A. Sharif[‡]

[†]Department of Physics and [‡]Department of Mechanical Engineering, California State University, Los Angeles, California 90032, United States

ABSTRACT: We report first-principles calculations, using the full potential linear augmented plane wave method, on six lead halide semiconductors, namely, $CH_3NH_3PbI_3$, $CH_3NH_3PbBr_3$, $CsPbX_3$ (X = Cl, Br, I), and $RbPbI_3$. Exchange is modeled using the modified Becke−Johnson potential. With an appropriate choice of the parameter that defines this potential, an excellent agreement is obtained between calculated and experimental band gaps of the six compounds.
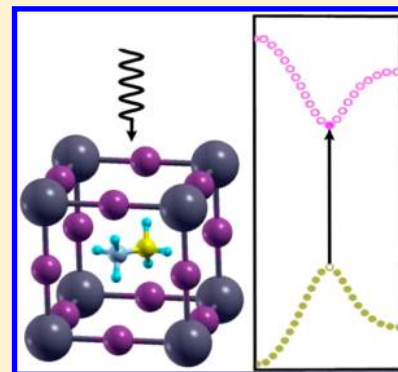
I. INTRODUCTION

Recently, materials with halide perovskite structure, with the general formula ABX_3, have attracted great interest, primarily because of their potential applications as light harvesters in solar cells[1] and as topological insulators.[2,3] Many studies have ensued with the aim of both improving the performance of these materials in photovoltaic cells and understanding which physical parameters may determine the efficiencies.[4−23] For example, Lee et al.[16] report a solution-processable solar cell which uses a perovskite of mixed halide form, namely, methylammonium lead iodide chloride, $CH_3NH_3PbI_2Cl$ (abbreviated as $MAPbI_2Cl$), with a solar-to-electrical power conversion efficiency of 10.9%. Using chemically tuned $MAPb(I_{(1−x)}Br_x)_3$ perovskites as light harvesters, a mesoporous titanium dioxide (TiO_2) film, and a hole-conducting polymer, Noh et al.[17] demonstrate solar cells with a 12.3% power conversion efficiency. Burschka et al.[18] describe a sequential deposition method whereby $MAPbI_3$ nanoparticles are formed within porous TiO_2, resulting in a power conversion efficiency of 15%. Liu et al.[19] have subsequently shown that such nanostructuring is not necessary for high efficiencies; a planar heterojunction solar cell, with a deposited thin film of $MAPbI_2Cl$ acting as a light absorber, can achieve an efficiency exceeding 15%. Umari et al.[15] and Even et al.[20−22] had emphasized the effect of spin−orbit coupling on the electronic structure of these materials.

$MAPbI_3$ and similar compounds are derived from a class of trihalide perovskite structures with the formula ABX_3 (A = Cs, Rb; B = Pb; X = Cl, Br, I) by replacing the alkali-metal atom with methylammonium (MA). Such a replacement causes a large downshift in the semiconducting energy gap, making the compounds useful for photovoltaic applications. It is anticipated that different band gaps may be obtained by replacing methylammonium with other entities such as NH_4 or CH_2CH,

by applying pressure, or by using thin films consisting of only a few layers.

To maximize the usefulness of such materials in photovoltaic applications, it is important to begin by developing computational techniques that accurately describe their electronic structure. Density functional theory in the Kohn−Sham formulation[24] is the most widely used method. Here, the exchange-correlation potential is approximated by a functional of the electronic density. The most common approximations are the local density approximation (LDA),[24] the generalized gradient approximation (GGA),[25] and the hybrid approximation.[26]

While LDA and GGA provide a successful description of ground-state properties in crystals, this success does not extend to a description of excited states. In many semiconductors, LDA and GGA strongly underestimate the value of the energy gap. Improved values for the band gaps are usually obtained by using the GW method.[27] However, the high computational cost of this method limits its applicability to crystals with a small number of atoms in the unit cell.

An exchange potential was recently proposed by Becke and Johnson (BJ), designed to yield the exact exchange potential in atoms.[28] Unfortunately, the use of this potential led to a slight improvement in the energy gap values for many semiconductors.[29] A simple modification of the BJ potential was proposed by Tran and Blaha.[30] In this method, known as TB-mBJ, the exchange potential is given by

$$V_x^{\text{TB-mBJ}}(\mathbf{r}) = cV_x^{\text{BR}}(\mathbf{r}) + (3c - 2)\frac{1}{\pi}\sqrt{\frac{5}{12}}\left[2t(\mathbf{r})/\rho(\mathbf{r})\right]^{1/2}$$

(1)

where $\rho(\mathbf{r})$ is the electron density, $t(\mathbf{r})$ the Kohn−Sham (KS) kinetic energy density, and $V_x^{BR}(\mathbf{r})$ the Becke−Roussel exchange potential.[31] In the TB-mBJ potential given in eq 1

$$c = A + B\sqrt{g} \tag{2}$$

where

$$g = \frac{1}{\Omega} \int \frac{1}{2} \left(\frac{|\nabla \rho_\uparrow(\mathbf{r})|}{\rho_\uparrow(\mathbf{r})} + \frac{|\nabla \rho_\downarrow(\mathbf{r})|}{\rho_\downarrow(\mathbf{r})} \right) d^3r \tag{3}$$

is the average of $|\nabla \rho / \rho|$ over the unit cell of volume Ω. The parameters $A = -0.012$ and $B = 1.023$ bohr$^{1/2}$ were chosen because they produce the best fit to the experimental band gaps of many semiconductors. Studies have shown that the TB-mBJ potential is generally as accurate in predicting the energy gaps of many semiconductors as the much more expensive GW method.[32]

Despite its many successes, however, the performance of the TB-mBJ method is not very satisfactory in certain cases, especially for transition metal oxides. To improve the band gap prediction, Koller, Tran, and Blaha[33] consider a more general form for c

$$c = A + Bg^e \tag{4}$$

They vary the values of parameters A, B, and e in order to improve the quality of the fit between the calculated and the experimental energy gaps of many semiconductors. There is an overall improvement in predicting the energy gaps of semiconductors with moderate gaps when $A = 0.267$, $B = 0.656$, and $e = 1$. The modified BJ method employing these values for A, B, and e will be referred to as the KTB-mBJ method. It should be pointed out that, in terms of computational time and resources, the requirements for the TB-mBJ and KTB-mBJ methods are essentially the same as those for standard LDA or GGA methods. Therefore, these methods may be easily used to calculate the electronic structure of crystals with large unit cells, where the cost of the GW method is prohibitive.

In this work, we present first-principles calculations on the electronic structure of six compounds, namely, $MAPbI_3$, $MAPbBr_3$, $CsPbX_3$ (X = Cl, Br, I), and $RbPbI_3$. All of these compounds have a perovskite structure, characterized by a Pb atom that is octahedrally coordinated to six halogen atoms. We show that GGA, when spin−orbit coupling (SOC) is included, severely underestimates the band gaps in these semiconducting materials. Though TB-mBJ and KTB-mBJ methods lead to significant improvement in the values of the gaps, both methods still underestimate the energy gaps by a wide margin. We then show that keeping parameters B and e essentially the same as in TB-mBJ, while adopting a new value for A, leads to results that are in excellent agreement with experimental values.

II. METHODS

Total energy and band structure calculations are carried out using the all-electron, full potential, linear augmented plane wave (FP-LAPW) method as implemented in the WIEN2k code.[34] Here, each atom is surrounded by a muffin-tin sphere, and the total space is divided into two regions. One region consists of the interior of these nonoverlapping spheres, while the rest of the space constitutes the interstitial region. The radii of the muffin-tin spheres are $2.5a_0$ for Cs, Rb, Pb, I, and Br, $2.37a_0$ for Cl, $1.27a_0$ for N, $1.33a_0$ for C, and $0.68a_0$ for H,

where a_0 is the Bohr radius. In GGA calculations, the exchange correlation potential is that proposed in ref 25.

The valence electrons' wave functions inside the muffin-tin spheres are expanded in terms of spherical harmonics up to $l_{max} = 10$. In the interstitial regions, they are expanded in terms of plane waves, with a wave vector cutoff of K_{max}. Because of the small muffin-tin radius of hydrogen atoms, we set $R_H K_{max} = 3$ in $CH_3NH_3PbI_3$ and $CH_3NH_3PbBr_3$, where $R_H = 0.68a_0$ is the muffin-tin radius of the H atom. In the remaining four compounds, we set $R_{mt}K_{max} = 9$, where R_{mt} is the smallest muffin-tin radius. The charge density is Fourier expanded up to a maximum wave vector of G_{max}, where $G_{max} = 20a_0^{-1}$ for $MAPbI_3$ and $MAPbBr_3$ and $G = 13a_0^{-1}$ for the remaining compounds. The convergence of the self-consistent calculations is achieved with a total energy tolerance of 0.1 mRy and a charge convergence of 0.001 e.

Additionally, the calculations on the cubic phase of $CsPbI_3$ were repeated using the GW method, as implemented within the FHI-gap code.[35] In carrying out these calculations, the wave vector cutoff K_{max} is the same as in the GGA calculations, and unoccupied states with an energy cutoff of 15 Ry are used. For the integration over the Brillouin zone, a mesh of 4 × 4 × 4 k-points is used, and in the GW_0 calculations, energy convergence is achieved with a tolerance of 0.1 mRy.

III. RESULTS AND DISCUSSION

At high temperatures, lead halide perovskites have a simple cubic unit cell, where Pb sits at the center of the cube and is octahedrally coordinated to six halogen atoms, while alkali atoms sit at the cube corners, as shown in Figure 1. As the
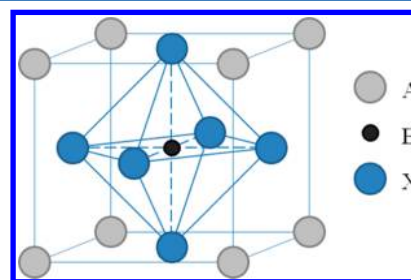
Figure 1. Cubic perovskite structure with alkali atoms occupying the A sites, Pb atoms occupying the B sites, and halogen atoms occupying the X sites.

temperature is lowered, distortions lead to tetragonal and/or orthorhombic structures. In our calculations, we use the room-temperature crystal structures of the various compounds. These are listed in Table 1. For $CsPbI_3$, which is orthorhombic at

Table 1. Crystal Structure and Lattice Constants for the Compounds Studied in This Work

compound	structure	lattice constants (Å)
$CH_3NH_3PbI_3$	tetragonal	$a = 8.856$, $c = 12.655^a$
$CH_3NH_3PbBr_3$	cubic	$a = 5.933^b$
$CsPbCl_3$	cubic	$a = 5.605^c$
$CsPbBr_3$	orthorhombic	$a = 8.244$, $b = 11.735$, $c = 8.198^d$
$RbPbI_3$	orthorhombic	$a = 10.276$, $b = 4.779$, $c = 17.393^e$
$CsPbI_3$	orthorhombic	$a = 10.458$, $b = 4.801$, $c = 17.776^e$
$CsPbI_3$	cubic	$a = 6.2894^e$

^{a}Poglitsch and Weber.[36] ^{b}Mashiyama et al.[37] ^{c}Moreira and Dias.[38] ^{d}Stoumpos et al.[39] ^{e}Trots and Myagkota.[40]

Table 2. Calculated and Experimental Band Gaps, in eV, for the Compounds That Are Studied in This Work[a]

compound	GGA	GGA+SOC	TB-mBJ	KTB-mBJ	present	GW	experiment
$CH_3NH_3PbI_3$	1.492	0.377	0.844	0.921	1.544	1.67[b,c]	1.5−1.6[d,e]
$CH_3NH_3PbBr_3$	1.668	0.453	1.183	1.406	2.233	-	2.28[d]
$CsPbCl_3$	2.498	0.707	1.585	1.889	2.829	-	2.86[f]
$CsPbBr_3$	1.794	0.669	1.316	1.461	2.228	-	2.24[f,g]
$RbPbI_3$	2.468	1.828	2.387	2.446	3.302	-	3.17[h]
$CsPbI_3$	2.504	1.876	2.426	2.476	3.330	-	3.14[h]
$CsPbI_3$ (cubic)	1.324	0.072	0.485	0.529	1.072	-	-

[a]The band gaps obtained by using parameters in eq 5 are reported under "Present". The TB-mBJ, KTB-mBJ, Present, and GW calculations all take into account the effect of spin−orbit coupling (SOC). [b]Umari et al.[15] [c]Brivio et al.[41] [d]Noh et al.[17] [e]Baikie et al.[42] [f]Liu et al.[43] [g]Stoumpos et al.[39] [h]Yunakova et al.[44]

room temperature, we also study the high-temperature cubic phase, which was predicted to be a topological insulator when subjected to hydrostatic pressure.[2]

We carried out band structure calculations on the six compounds shown in Table 1. Using GGA, we found that, upon including the effect of SOC, the band gaps of all compounds are severely underestimated. The values of the gaps are improved by using the TB-mBJ method and are improved further by using the KTB-mBJ method. However, the improvement does not go far enough, and the gaps are still far below the experimental values. We thus considered a new set of values for the parameters that appear in eq 4, namely

$$A = 0.4, \quad B = 1.0, \quad e = 0.5 \qquad (5)$$

The parameters B and e are essentially the same as in the TB-mBJ method, but the parameter A is different. With this new set of values for A, B, and e, the calculated band gaps of all six compounds are in excellent agreement with the experimental values. Our results are summarized in Table 2 where we present the band gaps calculated by using different methods. The gaps obtained by using the above values for A, B, and e are given in the column labeled 'Present'.

The calculated energy bands of MAPbI$_3$ along high symmetry directions in the Brillouin zone (BZ), in addition to the electronic density of states, are presented in Figure 2. The valence band maximum (VBM) and conduction band minimum (CBM) occur at the Γ-point, the BZ center. In cubic perovskites, the gap occurs at point $R(1/2, 1/2, 1/2)$. However,
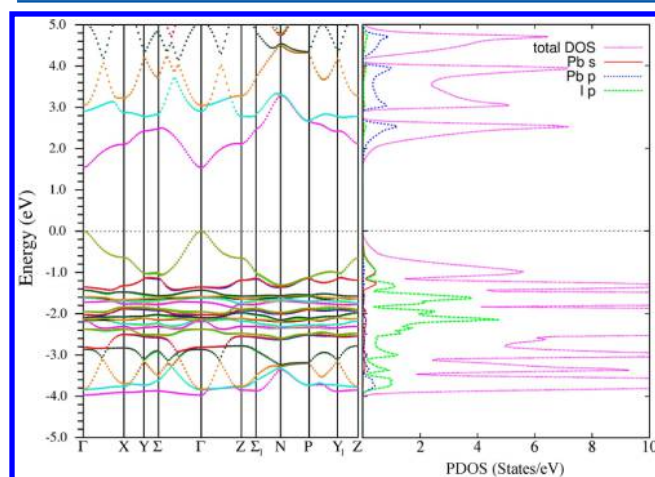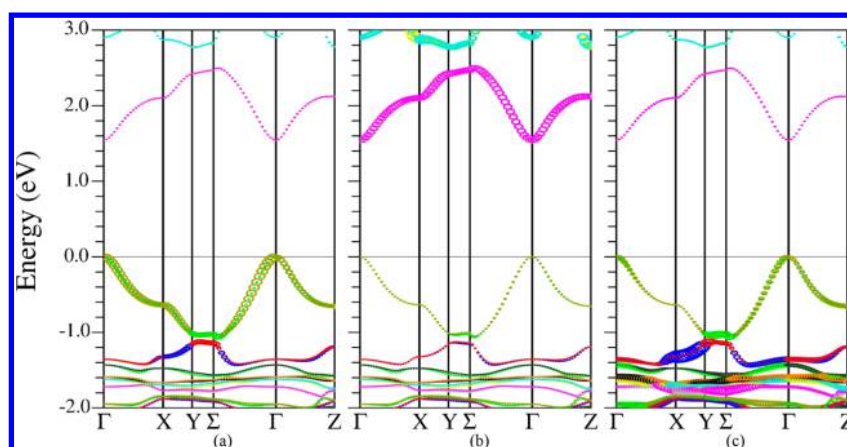
at room temperature, MAPbI$_3$ has a body-centered tetragonal crystal structure with two formula units per primitive cell. Its conventional unit cell, containing four formula units, is a slightly distorted $\sqrt{2} \times \sqrt{2} \times 2$ supercell of the high-temperature cubic phase unit cell. The distortion consists mainly of a rotation of the octahedron by 10.45° about the c-axis. Point R of the cubic lattice BZ is zone-folded into the Γ-point of the body-centered tetragonal lattice BZ.

The density of states of MAPbI$_3$ is shown in Figure 2, where we see that the low-lying conduction bands are derived from Pb p states. On the other hand, the bands in the range −4 to −2 eV are dominated by iodine-derived states. The valence band just below the Fermi energy is derived from lead s and iodine p states. These observations become clear upon considering the atomic orbital character of the bands, which is presented in Figure 3. The size of the circles is indicative of the contribution of the chosen atomic orbital to the eigenstates at each k-point. The CBM is derived mostly from Pb $6p$ states. The VBM, on the other hand, is a mixture of Pb $6s$ and I $5p$ states. The antibonding state formed from these s and p states is pushed up in energy close to the Fermi level. The large contribution of Pb $6s$ ($l = 0$) states to the VBM and Pb $6p$ ($l = 1$) states to the CBM suggests that there are strong optical transitions between the VBM and CBM ($\Delta l = 1$). This is in agreement with the results given by Filippetti and Mattoni.[45] Strong optical absorption, in conjunction with small electron and hole band masses,[45] is the reason behind the usefulness of these compounds for photovoltaic applications.

$CH_3NH_3PbBr_3$ (MAPbBr$_3$) has a cubic unit cell. Its band structure is shown in Figure 4, and as expected, the band gap occurs at point $R(1/2, 1/2, 1/2)$ in the Brillouin zone. As with the case of MAPbI$_3$, its VBM is a mixture of Pb $6s$ and Br $4p$ states, whereas its CBM is derived from Pb $6p$ states. In the absence of SOC, its CBM is 6-fold degenerate (including spin degeneracy). Due to SOC, its CBM is split into a doublet ($j = 1/2$) and a quartet ($j = 3/2$). The doublet is lowered in energy by an amount λ, whereas the quartet is raised in energy by $\lambda/2$, where $\lambda \approx 1.1$ eV. Similar perovskite structures, namely, CsSnX$_3$ (X = Cl, Br, I), where Sn replaces Pb, show a much smaller spin splitting of ∼0.4 eV.[46] Since the VBM is composed of Pb s and Br p orbitals, it is shifted slightly upward due to SOC on Br atoms. The large energy split of the CBM is, of course, due to the strong SOC on Pb atoms.

Finally, we consider the CsPbI$_3$ crystal. At high temperature (>634 K), the crystal is cubic, but at room temperature, it is strongly distorted to an orthorhombic structure. On the basis of LDA and sx-LDA calculations, it has been suggested that, under hydrostatic pressure, the cubic phase might become a topological insulator.[2] Calculations made using sx-LDA suggest
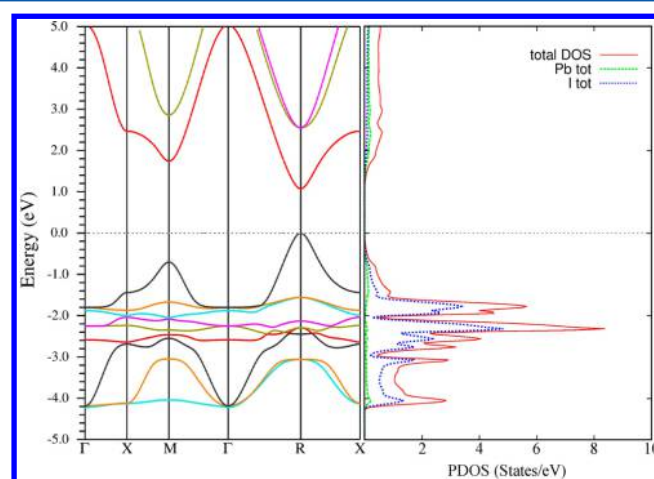

Figure 2. Band structure and density of states of $CH_3NH_3PbI_3$. These are obtained using the present parametrization of the mBJ potential, taking into account the effect of spin−orbit coupling.

Figure 3. Orbital character of the valence and conduction bands of $CH_3NH_3PbI_3$. The contribution of the selected orbital is proportional to the size of the circle, with a single point denoting zero contribution. (a) Pb 6s orbital, (b) Pb 6p orbital, and (c) I 5p orbital.
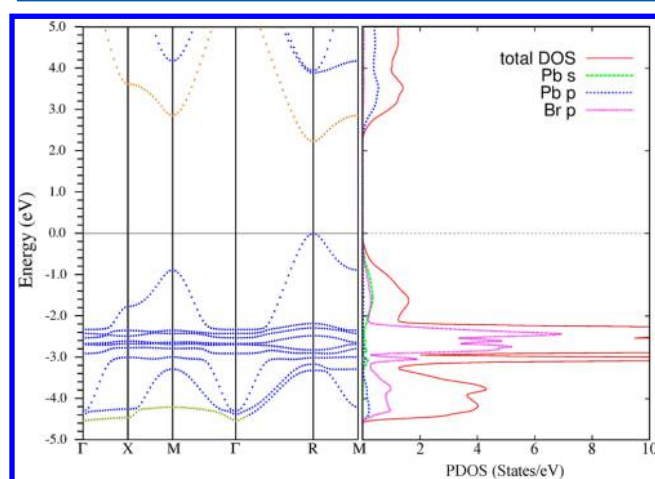
Figure 4. Band structure and partial density of states of $CH_3NH_3PbBr_3$. These are obtained using the present parametrization of the mBJ potential, taking into account the effect of spin−orbit coupling.

Figure 5. Band structure and partial density of states of cubic $CsPbI_3$. These are obtained using the present parametrization of the mBJ potential, taking into account the effect of spin−orbit coupling.

a gap of 0.566 eV for $CsPbI_3$ and 0.218 eV for $CsSnI_3$. With decreasing lattice constants, the bandwidth increases, and the band gap decreases; at some critical pressure, band inversion occurs.[2] However, GW calculations on $CsSnI_3$ give a much larger band gap of 1.008 eV.[46] Our calculations on the cubic phase of $CsPbI_3$ predict a band gap of 1.07 eV, larger by 0.5 eV than predicted by sx-LDA.

The band structure of cubic $CsPbI_3$ is shown in Figure 5. The band gap occurs at point R. As in the cases discussed previously, its CBM is derived from Pb 6p states, whereas its VBM is a mixture of Pb 6s and I 5p states. Without SOC, the calculated band gap is 2.27 eV, and the CBM is 6-fold degenerate (including spin degeneracy). SOC on Pb splits its CBM into a doublet ($j = 1/2$) and a quartet ($j = 3/2$). The doublet is lowered in energy by 1.1 eV, while the quartet is raised by 0.55 eV. On the other hand, SOC on the I atoms raises the VBM by 0.1 eV.

As a further check on our results for cubic $CsPbI_3$, we repeat the calculation of the band gap using the GW approximation within the linear augmented plane wave formalism.[35]

In this method, the electron's proper self-energy Σ^* is approximated as a product of the electron Green function (G) and an effective interaction term (W). In the absence of spin−

orbit coupling, we obtain band gap energies of 1.88 and 2.02 eV within the G_0W_0 and GW_0 approximations, respectively. This result is in good agreement with the value of 2.27 eV, which we obtain for the band gap, in the absence of SOC, upon using our present parametrization of the mBJ method. In the presence of SOC, we obtain band gap energies of 0.59 and 0.73 eV within the G_0W_0 and GW_0 methods, respectively. These values compare reasonably well with 1.07 eV (Table 2), the value obtained in this work.

In conclusion, we have presented electronic structure calculations on six lead halide compounds using the modified Becke−Johnson method. We used the experimental crystal structure of these compounds at room temperature. We found that by modifying the parameters that characterize the TB-mBJ method we obtain band gaps that are in excellent agreement with experiment. Using this new set of parameters, one should be able to predict the electronic structure of phases of these compounds that occur at different temperatures, as well as those of similar compounds obtained by replacing the alkali metal with various organic cations.

■ AUTHOR INFORMATION

Corresponding Author

*E-mail: radi.jishi@calstatela.edu.

■ REFERENCES

(1) Kojima, A.; Teshima, K.; Shirai, Y.; Miyasaka, T. Organometal Halide Perovskites as Visible-Light Sensitizers for Photovoltaic Cells. *J. Am. Chem. Soc.* **2009**, *131*, 6050−6051.

(2) Jin, H.; Im, J.; Freeman, A. J. Topological Insulator Phase in Halide Perovskite Structures. *Phys. Rev. B* **2012**, *86*, 121102.

(3) Yang, K.; Setyawan, W.; Wang, S.; Nardelli, M. B.; Curtarolo, S. A Search Model for Topo- logical Insulators with High-Throughput Robustness Descriptors. *Nat. Mater.* **2012**, *11*, 614−619.

(4) Etgar, L.; Gau, P.; Xue, Z.; Peng, Q.; Chandiran, A. K.; Liu, B.; Nazeeruddin, M. K.; Grätzel, M. Mesoscopic $CH_3NH_3PbI_3/TiO_2$ Heterojunction Solar Cells. *J. Am. Chem. Soc.* **2012**, *134*, 17396−17399.

(5) Ball, J. M.; Lee, M. M.; Hey, A.; Snaith, H. J. Low-Temperature Processed Meso- Superstructured to Thin-Film Perovskite Solar Cells. *Energy Environ. Sci.* **2013**, *6*, 1739−1743.

(6) Heo, H. J.; Im, S. H.; Noh, J. H.; Mandal, T. N.; Lim, C.-S.; Chang, J. A.; Lee, Y. H.; Kim, H.-j.; Sarkar, A.; Nazeeruddin, Md. K.; Grätzel, M.; Seok, S. I. Efficient Inorganic-Organic Hybrid Heterojunction Solar Cells Containing Perovskite Compound and Polymeric Hole Conductors. *Nat. Photonics* **2013**, *7*, 486−491.

(7) Kim, H.-S.; Lee, J.-W.; Yantara, N.; Biox, P. B.; Kulkarni, S. A.; Mhaisalker, S.; Grätzel, M.; Park, N.-G. High Efficiency Solid-State Sensitized Solar Cell-Based on Submicrometer Rutile TiO_2 Nanorod and $CH_3NH_3PbI_3$ Perovskite Sensitizer. *Nano Lett.* **2013**, *13*, 2412−2417.

(8) Bi, D.; Yang, L.; Boschloo, G.; Hagfeldt, A.; Johansson, E. M. J. Effect of Different Hole Transport Materials on Recombination in $CH_3NH_3PbI_3$ Perovskite-Sensitized Mesoscopic Solar Cells. *J. Phys. Chem. Lett.* **2013**, *4*, 1532−1536.

(9) Cai, B.; Xing, Y.; Yang, Z.; Zhang, W.-H.; Qiu, J. High Performance Hybrid Solar Cells Sensitized by Organolead Halide Perovskites. *Energy Environ. Sci.* **2013**, *6*, 1480−1485.

(10) Eperon, G. E.; Burlakov, V. M.; Docampo, P.; Goriely, A.; Snaith, H. J. Morphological Control for High Performance, Solution-Processed Planar Heterojunction Perovskite Solar Cells. *Adv. Funct. Mater.* **2014**, *24*, 151−157.

(11) Laban, W. A.; Etgar, L. Depleted Hole Conductor-Free Lead Halide Iodide Heterojunction Solar Cells. *Energy Environ. Sci.* **2014**, *6*, 3249−3253.

(12) Stranks, S. D.; Eperon, G. E.; Grancini, G.; Menelaou, C.; Alcocer, M. J. P.; Leijtens, T.; Herz, L. M.; Petrozza, A.; Snaith, H. J. Electron-Hole Diffusion Lengths Exceeding 1 Micrometer in an Organometal Trihalide Perovskite Absorber. *Science* **2013**, *342*, 341−344.

(13) Mosconi, E.; Amat, A.; Nazeeruddin, Md. K.; Grätzel, M.; De Angelis, F. First-Principles Modeling of Mixed Halide Organometal Perovskites for Photovoltaic Applications. *J. Phys. Chem. C* **2013**, *117*, 13902−13913.

(14) Wang, Y.; Gould, T.; Dobson, J. F.; Zhang, H.; Yang, H.; Yao, X.; Zhao, H. Density Func- tional Theory Analysis of Structural and Electronic Properties of Orthorhombic Perovskite $CH_3NH_3PbI_3$. *Phys. Chem. Chem. Phys.* **2014**, *16*, 1424−1429.

(15) Umari, P.; Mosconi, E.; De Angelis, F. Relativistic GW calculations on $CH_3NH_3PbI_3$ and $CH_3NH_3SnI_3$ Perovskites for Solar Cell Applications. *Scientific Reports* **2014**, *4*, Article number: 4467.

(16) Lee, M. M.; Teuscher, J.; Miyasaka, T.; Murakami, T. N.; Snaith, H. J. Efficient Hybrid Solar Cells Based on Meso-Superstructured Organometal Halide Perovskites. *Science* **2012**, *338*, 643−647.

(17) Noh, J. H.; Im, S. H.; Heo, J. H.; Mandal, T. N.; Seok, S. I. Chemical Management for Colorful, Efficient, and Stable Inorganic-Organic Hybrid Nanostructured Solar Cells. *Nano Lett.* **2013**, *13*, 1764−1769.

(18) Burschka, J.; Pellet, N.; Moon, S.-J.; Humphry-Baker, R.; Gao, P.; Nazeeruddin, M. K.; Grätzel, M. Sequential Deposition as a Route to High-Performance Perovskite-Sensitized Solar Cells. *Nature* **2013**, *499*, 316−319.

(19) Liu, M.; Johnston, M. B.; Snaith, H. J. Efficient Planar Heterojunction Perovskite Solar Cells by Vapour Deposition. *Nature* **2013**, *501*, 395−398.

(20) Even, J.; Pedesseau, L.; Jancu, J.-M.; Katan, C. Importance of Spin−Orbit Coupling in Hybrid Organic/Inorganic Perovskites for Photovoltaic Applications. *J. Phys. Chem. Lett.* **2013**, *4*, 2999−3005.

(21) Even, J.; Pedesseau, L.; Dupertuis, M.-A.; Jancu, J.-M.; Katan, C. Electronic Model for Self- Assembled Hybrid Organic/Perovskite Semiconductors: Reverse Band Edge Electronic States Ordering and Spin-Orbit Coupling. *Phys. Rev. B* **2012**, *86*, 205301.

(22) Even, J.; Pedesseau, L.; Katan, C. Comments On "Density Functional Theory Analysis of Structural and Electronic Properties of Orthorhombic Perovskite $CH_3NH_3PbI_3$". *Phys. Chem. Chem. Phys.* **2014**, *16*, 8697−8698.

(23) Feng, J.; Xiao, B. Correction to "Crystal Structures, Optical Properties, and Effective Mass Tensors of $CH_3NH_3PbI_3$ (X=I and Br) Phases Predicted from HSE06. *J. Phys. Chem. Lett.* **2014**, *5*, 1719−1720.

(24) Kohn, W.; Sham, L. J. Self-Consistent Equations Including Exchange and Correlation Effects. *Phys. Rev.* **1965**, *140*, A1133−A1138.

(25) Perdew, J. P.; Burke, K.; Ernzerhof, M. Generalized Gradient Approximation Made Simple. *Phys. Rev. Lett.* **1996**, *77*, 3865−3868.

(26) Becke, A. D. A New Mixing of Hartree-Fock and Local Density-Functional Theories. *J. Chem. Phys.* **1993**, *98*, 1372−1377.

(27) Bechstedt, F.; Fuchs, F.; Kresse, G. Ab-initio Theory of Semiconductor Band Structures: New Developments and Progress. *Phys. Status Solidi B* **2009**, *246*, 1877−1892.

(28) Becke, A. D.; Johnson, E. R. A Simple Effective Potential for Exchange. *J. Chem. Phys.* **2006**, *124*, 221101.

(29) Tran, F.; Blaha, P.; Schwarz, K. Band Gap Calculations with Becke-Johnson Exchange Potential. *J. Phys.: Condens. Matter* **2007**, *19*, 196208.

(30) Tran, F.; Blaha, P. Accurate Band Gaps of Semiconductors and Insulators with a Semilocal Exchange-Correlation Potential. *Phys. Rev. Lett.* **2009**, *102*, 226401.

(31) Becke, A. D.; Roussel, M. R. Exchange Holes in Inhomogeneous Systems: A Coordinate-Space Model. *Phys. Rev. A* **1989**, *39*, 3761−3767.

(32) Koller, D.; Tran, F.; Blaha, P. Merits and Limits of the Modified Becke-Johnson Exchange Potential. *Phys. Rev. B* **2011**, *83*, 195134.

(33) Koller, D.; Tran, F.; Blaha, P. Improving the Modified Becke-Johnson Exchange Potential. *Phys. Rev. B* **2012**, *85*, 155109.

(34) Blaha, P.; Schwarz, K.; Madsen, G. K. H.; Kvasnicka, D.; Luitz, J. *WIEN2K: An Augmented Plane Wave and Local Orbitals Program for Calculating Crystal Properties*; Schwarz, K., Ed.; Techn. Vienna University of Technology; Austria, 2001.

(35) Jiang, H.; Gomez-Abal, R. I.; Li, X.-Z.; Meisenbichler, C.; Ambrosch-Draxl, C.; Scheffler, M. FHI-gap: A GW Code Based on the All-Electron Augmented Plane Wave method. *Comput. Phys. Commun.* **2013**, *184*, 348−366.

(36) Poglitsch, A.; Weber, D. Dynamic Disorder in Methylammoniumtrihalogenoplumbates (II) Observed by Millimeter-Wave Spectroscopy. *J. Chem. Phys.* **1987**, *87*, 6373−6378.

(37) Mashiyama, H.; Kurihara, Y.; Azetsu, T. Disordered Cubic Perovskite Structure of $CH_3NH_3PbX_3$ (X=Cl,Br,I). *J. Korean Phys. Soc.* **1998**, *32*, S156−S158.

(38) Moreira, R. L.; Dias, A. Comment on "Prediction of Lattice Constant in Cubic Perovskites. *J. Phys. Chem. Solids* **2007**, *68*, 1617−1622.

(39) Stoumpos, C. C.; Malliakas, C. D.; Peters, J. A.; Liu, Z.; Sebastian, M.; Im, J.; Chasapis, T. C.; Wibowo, A. C.; Chung, D. Y.; Freeman, A. J.; Wessels, B. W.; Kanatzidis, M. G. Crystal Growth of the Perovskite Semiconductor CsPbBr$_3$: A New Material for High-Energy Radiation Detection. *Cryst. Growth Des.* **2013**, *13*, 2722−2727.

(40) Trots, D. M.; Myagkota, S. V. High-Temperature Structural Evolution of Caesium and Ru- bidium Triiodoplumbates. *J. Phys. Chem. Solids* **2008**, *69*, 2520−2526.

(41) Brivio, F.; Butler, K. T.; Walsh, A. Relativistic Quasiparticle Self-Consistent Electronic Structure of Hybrid Halide Perovskite Photovoltaic Absorbers. *Phys. Rev. B* **2014**, *89*, 155024.

(42) Baikie, T.; Fang, Y.; Kadro, J. M.; Schreyer, M.; Wei, F.; Mhaisalkar, S. G.; Graetzel, M.; White, T. J. Synthesis and Crystal Chemistry of the Hybrid Perovskite (CH$_3$NH$_3$)PbI$_3$ for Solid-State Sensitised Solar Cell Applications. *J. Mater. Chem. A* **2013**, *1*, 5628−5641.

(43) Liu, Z.; Peters, J. A.; Stoumpos, C. C.; Sebastian, M.; Wessels, B. W.; Im, J.; Freeman, A. J.; Kanatzidis, M. G. Heavy Metal Ternary Halides for Room-Temperature X-Ray and Gamma-Ray Detection. *Proc. SPIE* **2013**, *8852*, 88520A.

(44) Yunakova, O. N.; Miloslavskii, V. K.; Kovalenko, E. N. Exciton Absorption Spectrum of Thin (KI)$_{1−x}$(PbI$_2$)$_x$ films. *Funct. Mater.* **2013**, *20*, 59−63.

(45) Filippetti, A.; Mattoni, A. Hybrid Perovskites for Photovoltaics: Insights From First Principles. *Phys. Rev. B* **2014**, *89*, 125203.

(46) Huang, L. Y.; Lambrecht, W. R. L. Electronic Band Structure, Phonons, and Exciton Binding Energies of Halide Perovskites CsSnCl$_3$, CsSnBr$_3$, and CsSnI$_3$. *Phys. Rev. B* **2013**, *88*, 165203.